

RESEARCH

Open Access



Visualization of perivascular spaces in the human brain with 5-T magnetic resonance imaging

Sirui Liu^{1,2†}, Jianbo Li^{1,2†}, Rui Hua³, Yaowen Xing⁴, Jiaojiao Wu³, Jiang Lin^{1,2}, Jian Wang^{1,2}, Yan Shan^{1,2}, Lei Xu⁴, Feng Shi³ and Mengsu Zeng^{1,2*}

Abstract

Background To evaluate the effectiveness of 5-Tesla (T) magnetic resonance imaging (MRI) in the visualization of perivascular spaces (PVS).

Method A total of seventeen subjects underwent three-dimensional (3D) T1- and T2-weighted imaging on both 3-T and 5-T MRI systems. Twelve of these subjects underwent quantitative analysis of PVS in the semioval center (SOC) and basal ganglia (BG), with comparisons made between the two systems using paired-sample Wilcoxon tests. Additionally, high-resolution 5-T images were acquired for five other participants to examine the detailed anatomy of PVS in the SOC, BG, and cerebral cortex.

Results Compared with 3-T MRI, 5-T MRI detected more PVS in the SOC and BG [39.5 (32.0–63.0) vs. 56.5 (44.0–75.5) and 49.5 (27.0–55.8) vs. 65.5 (53.0–72.0)] with p -values of 0.002 and 0.004, respectively. In these two regions, the PVS tortuosity, defined as the ratio of the actual path length to the straight-line distance between the start and end points of the PVS, was lower at 3-T compared to 5-T ($p = 0.012$ for the SOC and $p = 0.006$ for the BG). The length of PVS in the SOC on 5-T was longer than those on 3-T [4.6 mm (3.9–6.3 mm) vs. 5.1 mm (4.6–6.7 mm), $p = 0.049$]. In addition, the 5-T MRI provided enhanced visualization of the morphology of PVS *in vivo*, and improved the depiction of PVS across various brain regions, especially in the cortex, illustrating their course and associated small vessels.

Conclusions 5-T MRI notably enhanced the visualization of PVS compared to 3-T, particularly in its ability to depict PVS anatomy in the cortex using high-resolution images. This advancement may pave the way for further research into the physiological roles of PVS and their involvement in related diseases.

Keywords 5-T, Magnetic resonance imaging, High resolution, Perivascular spaces

[†]Sirui Liu and Jianbo Li contributed equally to this work.

*Correspondence:

Mengsu Zeng

zeng.mengsu@zs-hospital.sh.cn

¹Department of Radiology, Zhongshan Hospital, Fudan University, No. 180 Fenglin Rd, Xuhui District, Shanghai 200032, China

²Shanghai Institute of Medical Imaging, Shanghai, China

³Department of Research and Development, United Imaging Intelligence Co., Ltd., 701 Yunjin Rd, Xuhui District, Shanghai 200232, China

⁴United Imaging Healthcare, No. 2258 Chengbei Rd, Jiading District, Shanghai 201807, China



Introduction

Perivascular spaces (PVS), also termed Virchow–Robin spaces, are interstitial fluid-filled cavities [1, 2] predominantly located in specific brain regions such as the basal ganglia (BG), the semioval center (SOC), the hippocampus, the midbrain, and the pons [3]. Among these, PVS in the BG and SOC have drawn increasing attention due to their associations with distinct diseases. For instance, PVS in the BG are often linked to cardiovascular diseases and risks [3, 4], whereas PVS in the SOC are associated with cerebral amyloid angiopathy (CAA) and Alzheimer's disease [5, 6]. These differences may reflect regional anatomical variations in PVS [6], yet the underlying pathophysiological mechanisms remain poorly understood.

A major obstacle to understanding PVS is their small size, which limits clear *in vivo* visualization [7–9]. Normal PVS are typically 0.13–0.96 mm in diameter, with most being smaller than 0.5 mm [10]. On conventional 1.5-T MRI, PVS visibility is often restricted to dilated structures (>2 mm) [11]. The advent of 3-T MRI has significantly improved the visualization of both normal and dilated PVS, while 7-T MRI has further advanced this capability. With its higher signal-to-noise ratio (SNR) (more than double that achievable with a 3-T MRI system) and increased spatial resolution, 7-T MRI enables the detection of smaller PVS (<1 mm) and facilitates more detailed anatomical studies [12]. Despite these advancements, challenges remain. Previous studies using 7-T MRI have described the morphology of PVS in various brain regions, but capturing cortical PVS *in vivo* remains difficult [7, 9, 13] due to their small size and insufficient spatial resolution [9]. As far as we know, detailed PVS images have not been obtained even at 7-T. Autopsy studies and *ex vivo* 7-T MRI have confirmed the presence of cortical PVS [8, 13]; however, this method lacks physiological relevance, as they do not reflect *in vivo* conditions.

The development of 5-T MRI systems offers a new avenue for studying small brain arteries, providing a balance between ultra-high-field imaging capabilities and clinical feasibility [14]. However, the gains in PVS visualization afforded by 5-T MRI remain largely unexplored. Given the clinical significance of PVS in the BG and SOC and the challenges associated with cortical PVS visualization, further investigation into the potential of 5-T MRI is warranted.

To address these gaps, this study employed a two-tiered approach. First, we assessed the clinical feasibility of 5-T MRI by comparing its performance to the widely used 3-T MRI under clinically acceptable scanning conditions. Second, we leveraged the high-resolution capabilities of 5-T MRI to explore the detailed anatomical structures of PVS and their surroundings.

Materials and methods

Study design

Study participants

This prospective study was approved by the institutional review board of Zhongshan Hospital, Fudan University, Shanghai, China (no. B2024-016R). Written informed consent was obtained from all participants. Seventeen healthy volunteers were recruited for the study. Based on their preferences, 12 participants consented to undergo clinical routine scanning using both 3-T and 5-T MRI sequences, while 5 participants agreed to the longer-duration, high-resolution 5-T MRI scanning.

The inclusion criteria were [15]: (a) no medical history of psychiatric disorder, cognitive impairment, or central neural system disease; and (b) normal in physical examination of the central nervous system. The exclusion criteria included images with artifacts (e.g., motion artifacts, magnetic susceptibility artifacts, and dielectric effects). Real-time motion monitoring was employed during 5-T acquisitions to minimize motion artifacts. Additionally, participants were positioned comfortably, and foam padding was placed between the head and coil to further reduce movement and enhance scan stability. To mitigate the risk of dielectric artifacts, a 2-Transmit and 48-Receive head coil was used, optimizing signal reception and reducing potential interference.

MR Acquisitions

MRI data were collected on two scanners: (a) a 5-T MRI scanner (uMR Jupiter, United Imaging Healthcare) with a 48-channel transmit-receive head coil; and (b) a 3-T MRI scanner (uMR 880, United Imaging Healthcare) with a 64-channel receive-only head coil.

Clinically appropriate 3-T and 5-T MRI protocols for comparison

To assess whether 5-T MRI offers additional benefits over 3-T MRI in visualizing PVS within practical scanning durations, we employed two clinically acceptable and commonly used whole-brain imaging sequences: (a) a whole-brain T2-weighted 3-dimensional (3D)-variable flip-angle fast spin-echo (FSE) sequence, and (b) a whole-brain T1-weighted 3D fast spoiled gradient echo (FSP) sequence. To ensure clinical relevance, we optimized parameters to maximize the performance of 3-T MRI while maintaining appropriate scan times. Comparable parameters were applied to 5-T MRI without extending the scanning duration. Detailed imaging protocols are provided in Table 1.

High-resolution 5-T MRI protocols for better visualization

Due to the small size of PVS, standard clinical imaging protocols may not fully capture their *in vivo* state. To address this limitation, we used high-resolution imaging

Table 1 Imaging protocols for visualizing and quantifying PVS on 5-T and 3-T MRI

Aims	Comparison of PVS				Visualization of PVS	
	3-T		5-T		5-T	
Field strength	3-T		5-T		5-T	
Sequence name	T1W_3D_FSP	T1W_3D_FSP	T2W_3D_FSE	T2W_3D_FSE	T1W_3D_FSP	T2W_3D_FSE
TR (ms)	7.8	10.4	2077	3000	7.4	3000
TE (ms)	3	3.5	271.44	420	2.5	422.82
FA (°)	9	10	66	60	9	56
FOV (mm)	230 × 256	240 × 240	224 × 224	240 × 256	224 × 224	220 × 260
Slice thickness (mm)	1	0.5	0.5	0.8	1	0.6
TA (min: s)	2:25	22:23	24:26	4:27	1:46	3:30

PVS: perivascular spaces, T1W_3D_FSP: T1-weighted 3-dimensional fast spoiled gradient echo, T2W_3D_FSE: T2-weighted 3-dimensional variable flip-angle fast spin-echo, FA: flip angle, FOV: field of view, TA: acquisition time, TE: echo time, TI: inversion time, TR: repetition time

(0.5-mm isotropic resolution) with extended but tolerable scan times (~50 min) to explore the full potential of 5-T MRI for detailed anatomical visualization of PVS. Detailed imaging protocols are provided in Table 1.

Imaging analysis

Assessment of PVS

The scoring system used to visualize PVS quality in BG and SOC was a ten-point scale (0 = PVS invisible; 10 = excellent depiction, PVS clearly visualized and PVS-tissue contrast appears high). Two radiologists, with 8 and 22 years of experience (SR L and Y S), independently performed the evaluations. Both radiologists were blinded to the MRI field strength and spatial resolution during their assessments.

The reproducibility of the image analysis was assessed through intra- and inter-observer studies. To avoid bias, images were reviewed by one reader (SR L) twice with an interval of two weeks. The same MRI scans were independently reviewed by another reader (Y S) for testing the inter-observer agreement during the first time measured by the first reader.

Three radiologists with 8, 18, and 22 years of experience (SR L, J W, and Y S) evaluated the course of PVS and its relationship with adjacent structures. They discussed their assessments to reach a consensus for each case.

Segmentation and quantification of PVS using clinically appropriate 3-T and 5-T images

Firstly, to acquire segmentation results of PVS, clinically appropriate T2-weighted sequences were transmitted to the uAI research portal (uRP, United Imaging Intelligence) [16], which integrates various segmentation and quantification models for calculating morphological features. Secondly, the automated segmentation results were checked and manually corrected on bilateral SOC and BG using ITK-SNAP 4.2.0 software (Cognitica, Philadelphia, PA, USA). PVS on MRI were identified by their signal and morphological characteristics [4]: exhibiting cerebrospinal fluid-like signals (hyperintense on T2

and hypointense on T1); having a linear, round, or ovoid shape; with a clear boundary; and no mass effect.

After manual correction, the number, length, tortuosity, and volume of PVS in the BG and SOC were evaluated. Here, the number refers to the total count of independent PVS detected in each region. Length represents the average length of the PVS, quantified based on its skeleton and measured in millimeters (mm). Tortuosity refers to the average PVS tortuosity, calculated as the ratio of the actual path length to the straight-line distance between the start and end points of the PVS, making it a dimensionless measure. Volume indicates the total PVS volume within each region and is expressed in cubic centimeters (mm³).

Visualization of PVS on high-resolution 5-T images

For each area, we studied: (a) the shape features of PVS; (b) their association with related arteries and veins; and (c) their connections with cisterns and ventricles. To achieve this, 3D T1-weighted and T2-weighted MR images were studied in 3 orientations (sagittal, transverse, and coronal). The transverse and coronal directions of slices were reformatted from the original data.

Vessels associated with PVS were defined as follows: (a) linear structures with hypointensity on T2-weighted images; (b) originating from the anterior or middle cerebral artery, or draining into the cerebral venous sinus; (c) located within PVS. To better illustrate the course of small vessels, minimum intensity projections (minIPs) of T2-weighted images were utilized. MinIPs are a visualization technique that projects the lowest intensity values along a given viewing plane, creating a 2-dimensional image that highlights low-intensity structures within a 3D dataset, such as small vessels or fluid-filled spaces.

Statistical analysis

The statistical analysis was performed using SPSS (version 20; IBM, Inc., Armonk, NY, United States) and GraphPad Prism 10.3.0 for Windows (GraphPad Software, www.graphpad.com). Paired sample Wilcoxon tests were utilized to compare quantitative measurements of

PVS. Kruskal-Wallis H tests were used to test the scoring of PVS among groups. Inter- and intra-observer agreement was assessed using weighted kappa coefficients. Nonnormally distributed data were expressed as medians (interquartile ranges). Two-tailed $P < 0.05$ was considered indicative of a statistically significant difference.

Results

Comparison of PVS between 3-T and 5-T MR

Assessment of image quality of 3-T and 5-T images

The image quality of seventeen volunteers (11 males and 6 females, mean age: 33.9 ± 8.4 years old) was assessed. None of the images exhibited motion artifacts, magnetic susceptibility artifacts, or dielectric effects. The inter- and intra-observer agreements for PVS scoring were found to be excellent across all imaging modalities,

including clinically appropriate 3-T and 5-T sequences, as well as high-resolution 5-T sequences (Additional file 1). The qualitative image scores of PVS differed significantly among the sequences on 3-T and 5-T MRI (clinically appropriate 3-T vs. clinically appropriate 5-T vs. high-resolution 5-T; scores in BG: 6.0 (5.0–6.0) vs. 6.0 (6.0–7.8) vs. 10.0 (9.0–10.0), $p < 0.001$; scores in SOC: 5.5 (5.0–6.0) vs. 6.0 (6.0–7.8) vs. 10.0 (9.0–10.0), $p < 0.001$).

When using clinically appropriate sequences, PVS on 5-T MRI exhibited better continuity and clearer boundaries than on 3-T MRI (Fig. 1A, B), which improved segmentation accuracy (Fig. 2B, D, E, H). However, neither clinically appropriate 3-T nor 5-T MRI could depict cortical PVS (Fig. 1C, D). In addition, High-resolution 5-T images demonstrated sharper boundaries of PVS

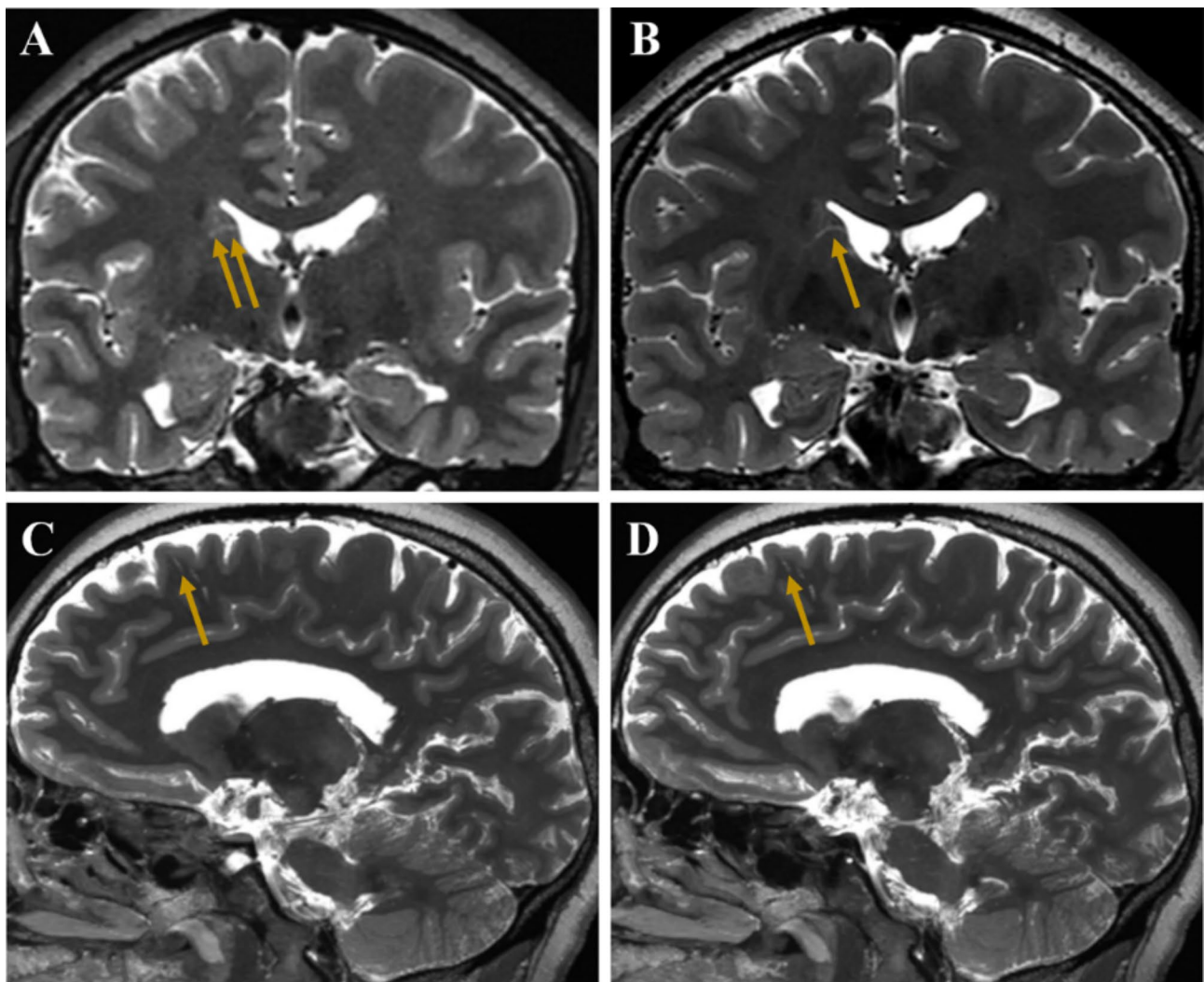


Fig. 1 Visual comparison of PVS between 3-T and 5-T MRI using clinically appropriate sequences. Representative slices of the same person's 3-T and 5-T MR images. **A** and **B** coronal T2-weighted images. **C** and **D** T2-weighted (4-mm mIP). Compared to 3-T (**A**) PVS in the head of the right caudate nucleus on 5-T (**B**) had better continuity and clearer boundaries (arrowhead). PVS in the frontal lobe terminate at the juxtacortical region without extending into the cortex on 3-T (**C**) and 5-T (**D**) images. PVS, perivascular spaces; MRI, magnetic resonance imaging; mIP, maximum intensity projection

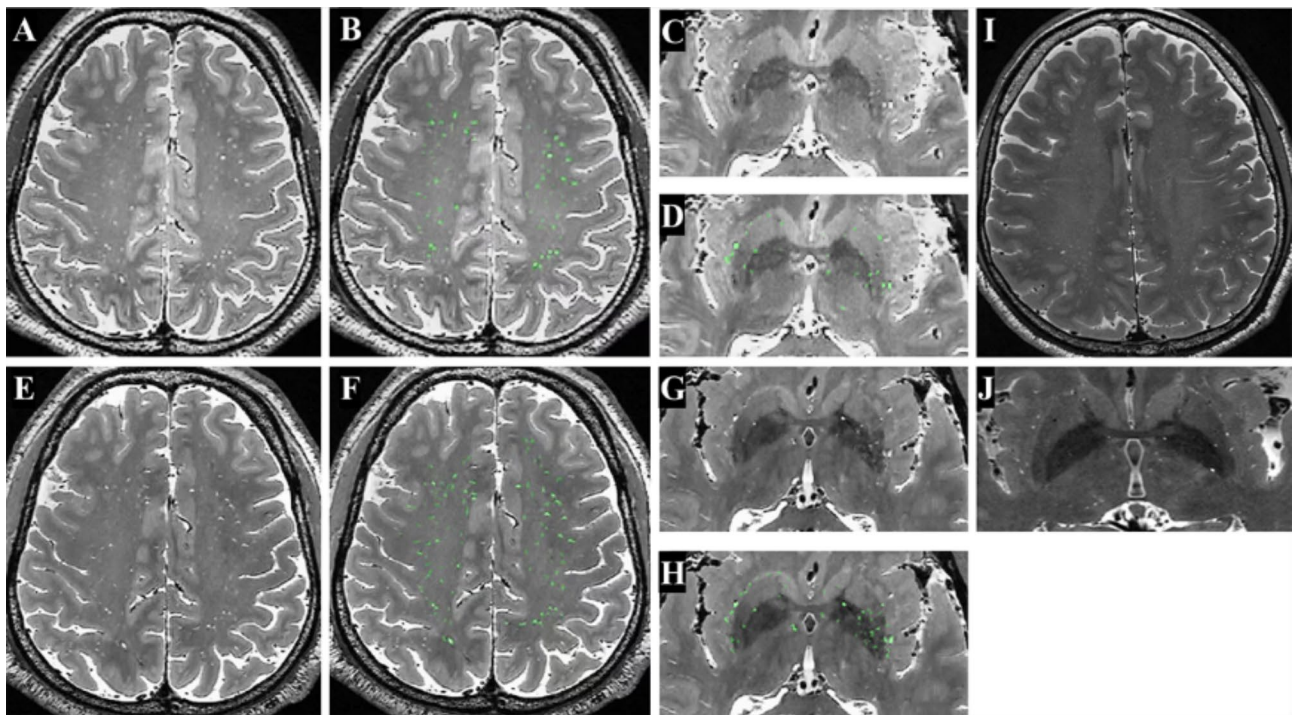


Fig. 2 Segmentation and visualization of PVS on the 3-T and 5-T MRI. **A** and **C** axial T2-weighted images on 3-T from a healthy 53-year-old male. **E** and **G** equivalent clinically appropriate T2-weighted 5-T slices acquired from the same volunteer showed more PVS than 3-T. **B** and **D**, PVS segmentation results on 3-T, which show overestimation, particularly for the smaller PVS. **F** and **H** PVS segmentation results on 5-T, with improved accuracy. **I** and **J** axial high-resolution T2-weighted images on 5-T from a healthy 50-year-old male reveal sharper boundaries and greater clarity than both 3-T and clinically appropriate 5-T sequences. PVS, perivascular spaces; MRI, magnetic resonance imaging

Table 2 Comparison of quantitative measurements of PVS between 5-T and 3-T MRI

	3-T	5-T	P-value
PVS in the semioval center			
Number	39.5 (32.0–63.0)	56.5 (44.0–75.5)	0.002*
Length (mm)	4.6 (3.9–6.3)	5.1 (4.6–6.7)	0.049*
Tortuosity	1.5 (1.4–1.7)	1.8 (1.7–2.2)	0.012*
Volume (mm ³)	477.6 (207.1–1099.9)	470.1 (297.8–1061.7)	0.347
PVS in the basal ganglia			
Number	49.5 (27.0–55.8)	65.5 (53.0–72.0)	0.004*
Length (mm)	5.8 (5.2–6.8)	5.8 (5.4–7.5)	0.272
Tortuosity	1.7 (1.6–2.1)	2.3 (2.0–2.6)	0.006*
Volume (mm ³)	752.0 (621.1–1139.8)	758.8 (556.6–1151.5)	0.875

PVS: perivascular spaces

Data were expressed as medians (interquartile ranges); * $P < 0.05$

compared to clinically appropriate 3-T and 5-T images (Fig. 2).

Quantitative comparison of PVS between clinically appropriate 3-T and 5-T sequences

Twelve participants (8 males and 4 females, mean age: 30.8 ± 7.4 years old) were included. Figure 2 shows the PVS segmentation results.

Table 2; Figs. 3, and 4 compare the quantitative features of PVS between 3-T and 5-T MRI. Compared to

3-T MRI, 5-T MRI detected more PVS in the SOC and BG regions [39.5 (32.0–63.0) vs. 56.5 (44.0–75.5) and 49.5 (27.0–55.8) vs. 65.5 (53.0–72.0); $p = 0.002$ and $p = 0.004$; respectively]. In these two regions, 3-T had statistically lower PVS tortuosity than 5-T [1.5 (1.4–1.7) vs. 1.8 (1.7–2.2) for the SOC, and 1.7 (1.6–2.1) vs. 2.3 (2.0–2.6) for the BG]. In addition, the length of PVS in the SOC on 5-T was longer than that on 3-T [4.6 mm (3.9–6.3 mm) vs. 5.1 mm (4.6–6.7 mm), $p = 0.049$]. However, the volume difference of PVS between these two scanners was not statistically significant.

Visualization of PVS on high-resolution 5-T images

To allow better observation of PVS, five participants (3 males and 2 females, mean age: 41.6 ± 5.0 years old) were included.

Semioval center and cerebral cortex

All subjects had PVS in the SOC on 5-T MRI. PVS were shaped as smooth arcs with relatively uniform diameters. PVS started 3 to 10 mm from the wall of the lateral ventricles, passed through the SOC, and then radiated to the frontal and parietal lobes in a direction parallel to the gyrus, some of which penetrated white matter along their way into the cortex (Fig. 5A, B). They had no connections with the lateral ventricles. PVS in the juxtacortical region

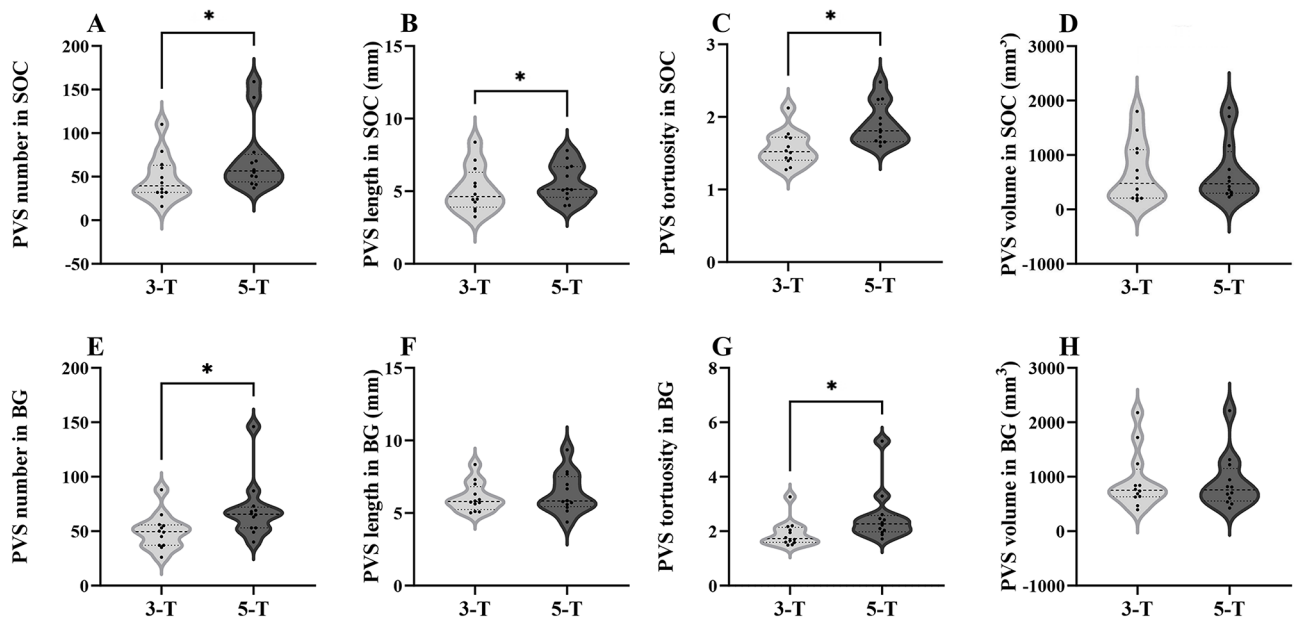


Fig. 3 Violin plots of quantitative measurements of PVS between 3-T and 5-T MRI. PVS number (A), length (B), tortuosity (C), and volume (D) in SOC. PVS number (E), length (F), tortuosity (G), and volume (H) in BG. PVS, perivascular spaces; MRI, magnetic resonance imaging; BG, basal ganglia; SOC, semioval center. * $P < 0.05$

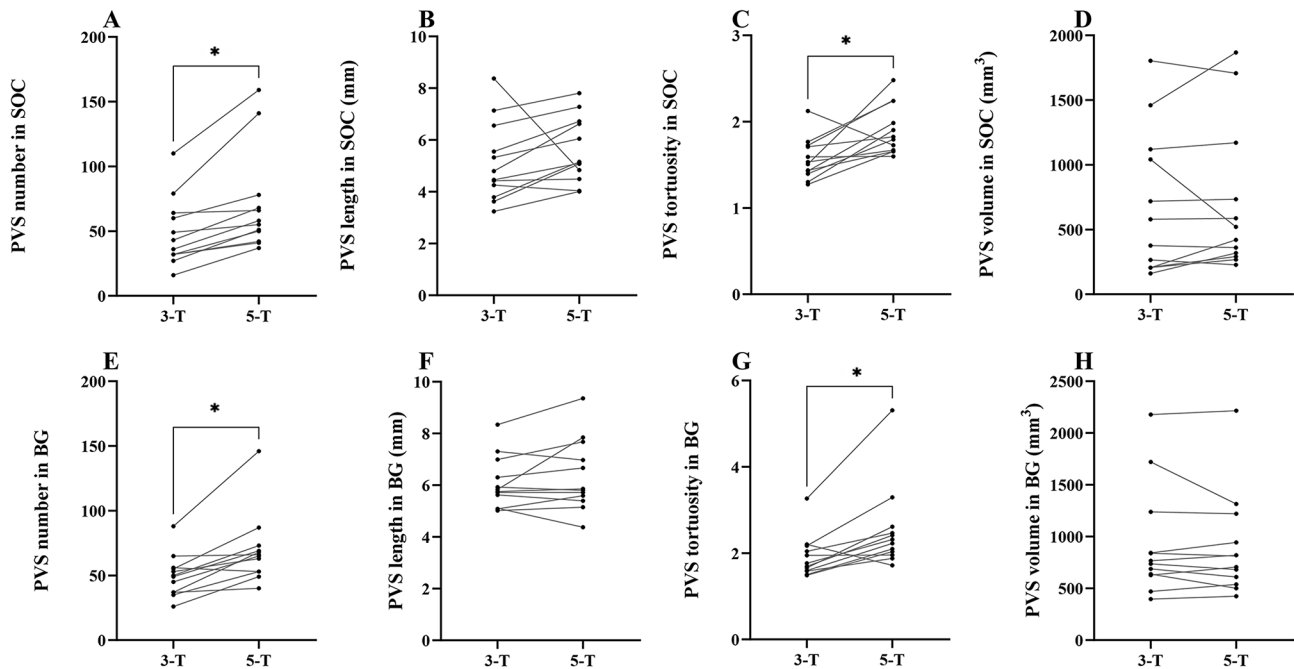


Fig. 4 Line plots of each individual's quantitative measurements of PVS between 3-T and 5-T MRI. PVS number (A), length (B), tortuosity (C), and volume (D) in SOC. PVS number (E), length (F), tortuosity (G), and volume (H) in BG. PVS, perivascular spaces; MRI, magnetic resonance imaging; BG, basal ganglia; SOC, semioval center. * $P < 0.05$

were seen. PVS around the venules were sometimes observed (Fig. 6).

Basal ganglia

PVS on 5-T MRI were seen throughout the BG in all subjects. PVS in the lower part of the BG moved along with

perforating arteries; they started from the basal cisterns; dilated in the lower third of the capsular nucleus with a length of 3 to 4 mm; and then tapered toward the caudate nucleus (Fig. 5D). The upper part of the BG had few PVS and were small in size. They gradually moved toward the outside of the lenticular nucleus (Fig. 5C). Connections

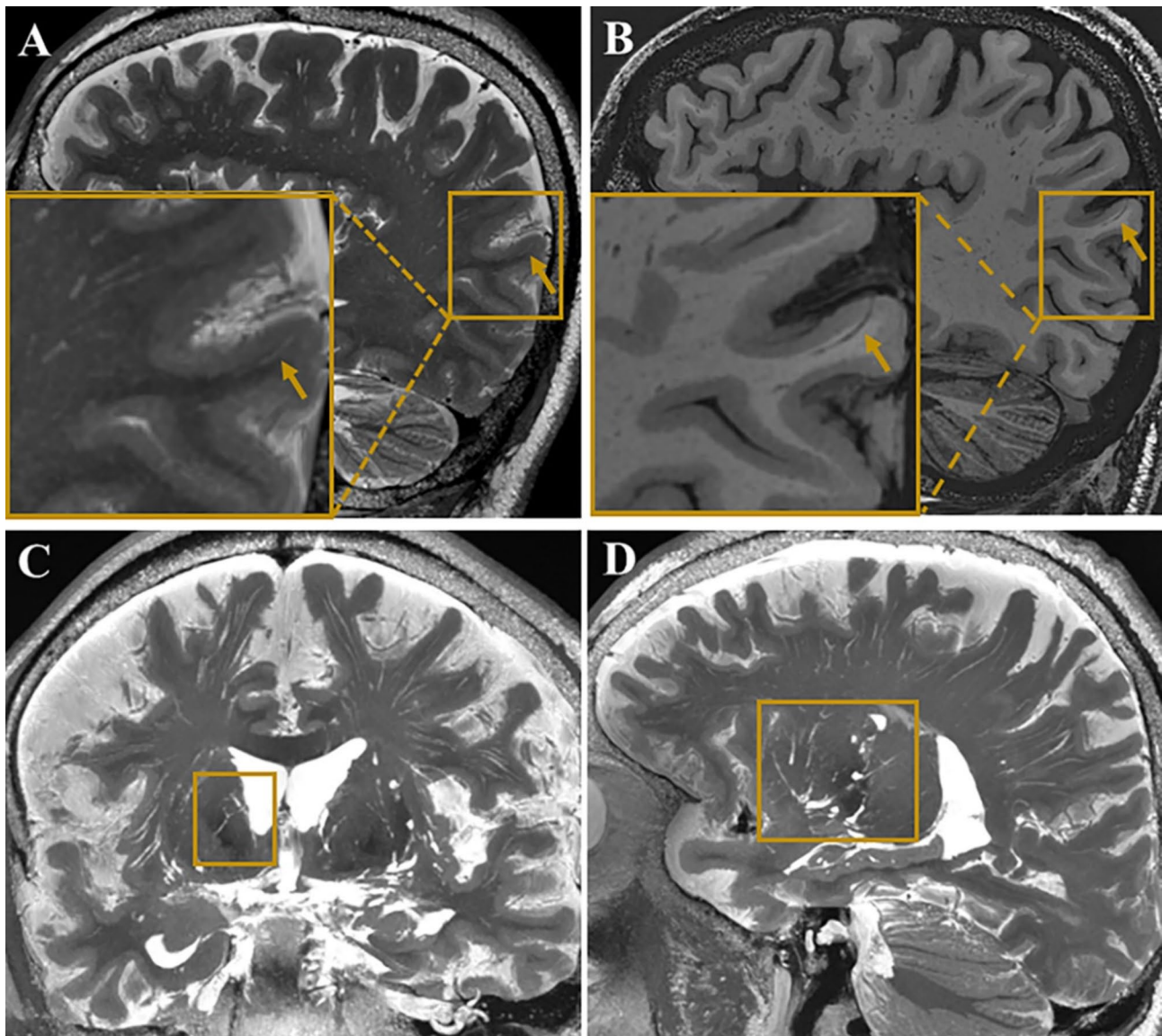


Fig. 5 High-resolution 5-T MRI visualization of perivascular spaces in the cerebral cortex and basal ganglia. **A** T2-weighted images. **B** T1-weighted images. **C** T2-weighted (11-mm mIP). **D** T2-weighted (8-mm mIP). **A** and **B** PVS in the white matter extended into the cortex (arrow). PVS in the upper part of the basal ganglia moved toward the outside of the lenticular nucleus (**C**). PVS in the lower part of the basal ganglia dilated at the beginning and then tapered toward the caudate nucleus (**D**). MRI, magnetic resonance imaging; PVS, perivascular spaces; mIP, maximum intensity projection

between PVS and the lateral ventricle were observed. Lenticulostriate arteries inside PVS were sometimes seen (Fig. 7).

Discussion

The present study first compared the ability of 3-T and 5-T MRI to display PVS *in vivo* under clinically available conditions. It then explored the full potential of high-resolution 5-T images for detailed anatomical visualization of PVS. This dual approach provides a balanced perspective on the clinical utility and imaging potential of 5-T MRI, advancing the understanding of PVS in both routine and high-resolution imaging contexts.

In this study, using the clinically feasible sequences, 5-T MRI detected more PVS in both the SOC and BG compared to 3-T MRI. The enhanced continuity of PVS visualization on 5-T contributed to longer measured lengths and higher tortuosity. Notably, the higher PVS volume observed with high-resolution 3-T sequences compared to prior studies [12, 17] may be attributed to thinner slice thickness and differences in participant demographics. Despite the improved resolution of 5-T MRI, the difference in PVS volume between 3-T and 5-T was not statistically significant. This discrepancy is likely due to the blurred boundaries of PVS on 3-T images, which can lead

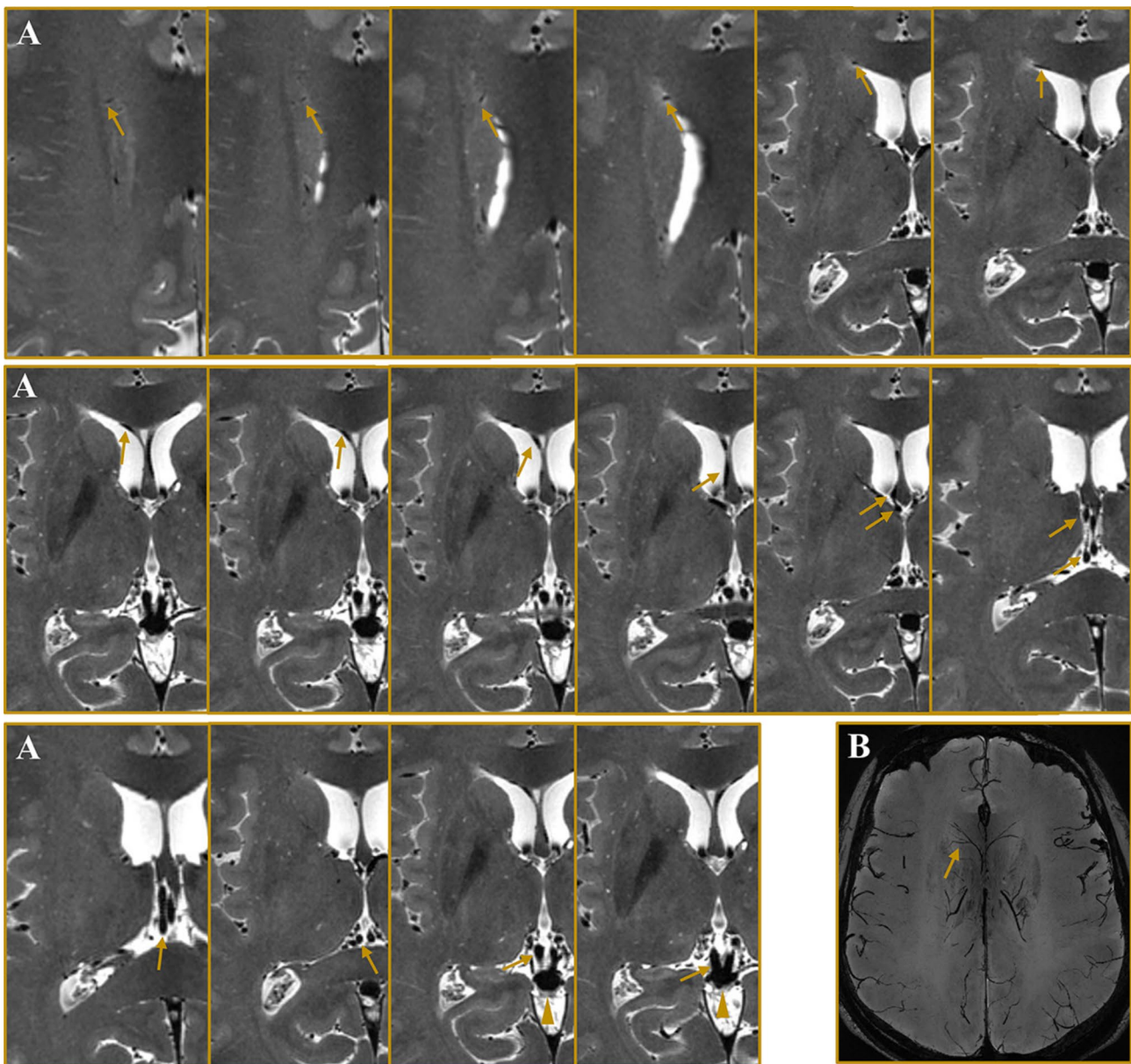


Fig. 6 Venules and inside PVS from a 50-year-old man. **A** T2-Weighted images (zoomed in to show right-hemisphere). **B** a T2-weighted (16-mm miniIP) image. An example of a venule's course (arrow) within PVS (**A** and **B**). The patent vein was a branch of the septal cerebral vein that drained into the straight sinus (arrowhead). PVS, perivascular spaces; miniIP: minimum intensity projection

to overestimation during segmentation, particularly for smaller PVS [11].

For a more detailed anatomical analysis of PVS, we employed a 0.5-mm isotropic high-resolution protocol on 5-T MRI, which provided deeper insights into PVS structural characteristics by offering sharper delineation of their boundaries compared to standard 3-T and 5-T clinical imaging. This high-resolution approach detected PVS extending into the cortex, a feature not observed in conventional clinical 3-T and 5-T scans, nor in previous *in vivo* 7-T studies [7, 9, 13]. The resolution used in this study (e.g., $0.7 \times 0.7 \times 0.7 \text{ mm}^3$) might not be high enough

to show subtle structures, so future studies using a higher resolution on 7 T MRI may be able to depict cortical PVS more clearly. 5-T MRI also had a good performance on PVS in the juxtacortical region, which was highly associated with CAA [13]. The observation of cortical and subcortical structures has always been the focus and difficulty of neuroscience research. The findings of our study suggested that the utilization of 5-T MR could improve the visualization of submillimeter-sized PVS.

Since the relationship between MRI-visible PVS and whether they surround arterioles, venules, or both remains under debate [3, 18], our study explored this

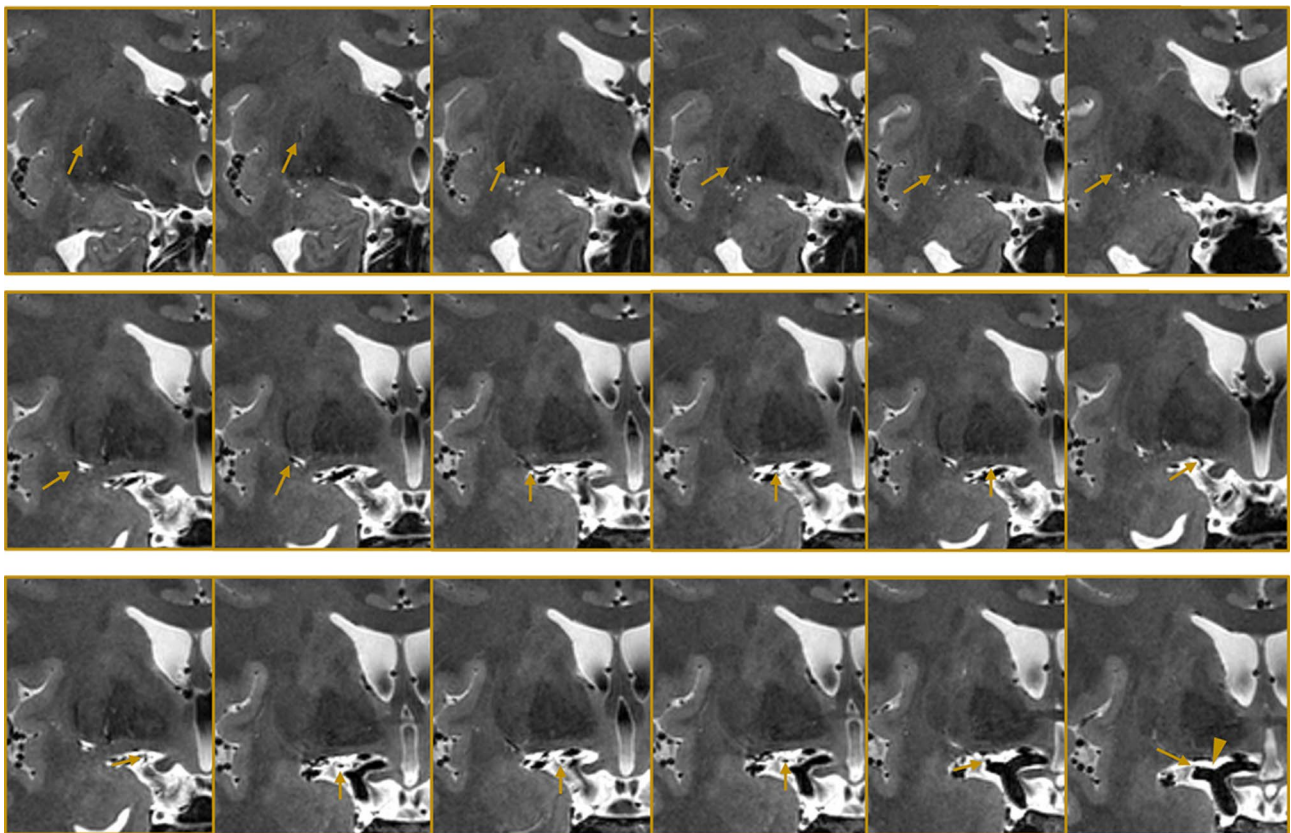


Fig. 7 An example of the perforating artery inside PVS. Representative slices of high-resolution T2-weighted images on 5-T from a 38-year-old man (magnified to show the right hemisphere). A lenticulostriate artery (arrow) originating from the middle cerebral artery (arrowhead) is observed within PVS in the right basal ganglia. PVS, perivascular spaces

aspect and observed the presence of arteries and venules within PVS in the basal ganglia and semioval center, respectively. This observation is consistent with previous 3-T and 7-T MRI studies [6, 18–20].

At present, the association between anatomic-specific changes of PVS (e.g., number, volume, location) and various disease states has been established [2, 19, 21–23]. Given that pathological changes in PVS were anticipated to commence at submillimeter scales [24], the utilization of 5-T MRI, which enhances the visibility of PVS in various brain regions, is fundamental not only for the detection of early and subtle pathological alterations of PVS but also for the analysis of physiological non-dilated PVS. However, the normal distribution and the pathogenic alterations of PVS in human brains are not yet fully understood, limiting the ability to confidently define PVS pathogenic alterations, especially in subclinical stages [11]. Therefore, identifying features of PVS helps distinguish between physiological and pathophysiological PVS, thereby providing insights into the diagnosis of various diseases related to PVS [11].

Although 3-T MRI has fewer physiologic considerations and B_1 inhomogeneity [25] compared to 5-T MRI, it is less effective in visualizing PVS in this study.

In theory, a higher magnetic field can give a higher SNR [14]. Previous studies [7, 11, 20, 26, 27] have shown that 7-T improves the accuracy of PVS visualization and quantitation. However, in our study, the ability to visualize PVS was not compared among all three MRI systems. Therefore, future studies should include direct comparisons of 3-T, 5-T, and 7-T MRI to fully assess the strengths and weaknesses of each system for PVS imaging.

This study had some limitations. First, the sample size was relatively small, but the number of PVS detected in each participant was high. In addition, the sample size was indeed in line with previous comparable studies using ultra-high field strength MRI [7, 14, 28]. Second, we did not compare the dataset with that at 7-T to tell more usefulness of 5-T MRI. Third, the sequences used to enhance the visualization of PVS required a relatively long acquisition time. Fourth, we evaluated PVS in pre-defined regions, which might not adequately reflect the distribution and morphological characteristics of PVS in the whole brain.

Conclusion

In conclusion, 5-T MRI enhanced the visualization of PVS in the human brain than 3-T MRI, especially in the cortex. Our findings extended the existing knowledge of PVS and contributed to an increased understanding of the neuroanatomy of PVS in the human brain.

Supplementary Information

The online version contains supplementary material available at <https://doi.org/10.1186/s12868-025-00925-z>.

Supplementary Material 1

Acknowledgements

We would like to acknowledge the reviewers for their helpful comments on this paper.

Author contributions

I confirm that all authors have made substantial contributions to all of the following: (1) the conception and design of the study (LSR, LJ, SY, and ZMS), or acquisition of data (LJB, XL, and XYW), or analysis and interpretation of data (LSR, LJB, HR, WJ, SF, and WJJ), (2) drafting the article (LSR and WJJ), (3) final approval of the version to be submitted (LSR, LJB, SF, HR, WJJ, XYW, XL, LJ, WJ, SY, and ZMS). All authors read and approved the final manuscript.

Funding

This work was supported by the National Natural Science Foundation of China (grant number: 82302157), and the National Key Research and Development Program of China (grant number: 2023YFF1204304).

Data availability

The datasets used and/or analyzed during this study are available from the corresponding author upon reasonable request.

Declarations

Ethical approval and consent to participate

This prospective study was approved by the institutional review board of Zhongshan Hospital, Fudan University (no. B2024-016R). Written informed consent was obtained from all participants.

Clinical trial number

Not applicable.

Consent for publication

Not applicable.

Competing interests

The authors declare no competing interests.

Received: 9 October 2024 / Accepted: 10 January 2025

Published online: 03 March 2025

References

- Arbel-Ornath M, Hudry E, Eikermann-Haerter K, Hou S, Gregory JL, Zhao L, Betensky RA, Frosch MP, Greenberg SM, Bacskaï BJ. Interstitial fluid drainage is impaired in ischemic stroke and Alzheimer's disease mouse models. *Acta Neuropathol.* 2013;126(3):353–64.
- Yakushiji Y, Charidimou A, Hara M, Noguchi T, Nishihara M, Eriguchi M, Nanri Y, Nishiyama M, Werring DJ, Hara H. Topography and associations of perivascular spaces in healthy adults: the Kashima scan study. *Neurology.* 2014;83(23):2116–23.
- Wardlaw JM, Benveniste H, Nedergaard M, Zlokovic BV, Mestre H, Lee H, Doubal FN, Brown R, Ramirez J, MacIntosh BJ, et al. Perivascular spaces in the brain: anatomy, physiology and pathology. *Nat Reviews Neurol.* 2020;16(3):137–53.
- Liu S, Hou B, You H, Zhang Y, Zhu Y, Ma C, Zuo Z, Feng F. The Association between Perivascular spaces and Cerebral Blood Flow, Brain volume, and Cardiovascular Risk. *Front Aging Neurosci.* 2021;13:599724.
- Banerjee G, Kim HJ, Fox Z, Jager HR, Wilson D, Charidimou A, Na HK, Na DL, Seo SW, Werring DJ. MRI-visible perivascular space location is associated with Alzheimer's disease independently of amyloid burden. *Brain.* 2017;140(4):1107–16.
- Oltmer J, Mattern H, Beck J, Yakupov R, Greenberg SM, Zwanenburg JJ, Arts T, Düzel E, van Veluw SJ, Schreiber S et al. Enlarged perivascular spaces in the basal ganglia are associated with arteries not veins. *J Cereb Blood flow Metabolism: Official J Int Soc Cereb Blood Flow Metabolism.* 2024;271678x241260629.
- Bouvy WH, Biessels GJ, Kuijf HJ, Kappelle LJ, Luijten PR, Zwanenburg JJ. Visualization of perivascular spaces and perforating arteries with 7 T magnetic resonance imaging. *Invest Radiol.* 2014;49(5):307–13.
- Marín-Padilla M, Knopman DS. Developmental aspects of the intracerebral microvasculature and perivascular spaces: insights into brain response to late-life diseases. *J Neuropathol Exp Neurol.* 2011;70(12):1060–9.
- Zong X, Park SH, Shen D, Lin W. Visualization of perivascular spaces in the human brain at 7T: sequence optimization and morphology characterization. *NeuroImage.* 2016;125:895–902.
- Pesce C, Carli F. Allometry of the perivascular spaces of the putamen in aging. *Acta Neuropathol.* 1988;76(3):292–4.
- Barisano G, Law M, Custer RM, Toga AW, Sepehrband F. Perivascular Space Imaging at Ultrahigh Field MR Imaging. *Magn Reson Imaging Clin N Am.* 2021;29(1):67–75.
- Hupfeld KE, Richmond SB, McGregor HR, Schwartz DL, Luther MN, Beltran NE, Kofman IS, De Dios YE, Riascos RF, Wood SJ, et al. Longitudinal MRI-visible perivascular space (PVS) changes with long-duration spaceflight. *Sci Rep.* 2022;12(1):7238.
- Perosa V, Oltmer J, Munting LP, Freeze WM, Auger CA, Scherlek AA, van der Kouwe AJ, Iglesias JE, Atzeni A, Bacskaï BJ, et al. Perivascular space dilation is associated with vascular amyloid- β accumulation in the overlying cortex. *Acta Neuropathol.* 2022;143(3):331–48.
- Shi Z, Zhao X, Zhu S, Miao X, Zhang Y, Han S, Wang B, Zhang B, Ye X, Dai Y, et al. Time-of-flight intracranial MRA at 3 T versus 5 T versus 7 T: visualization of distal small cerebral arteries. *Radiology.* 2022;305(3):E72.
- Liu S, Hou B, Zhang Y, Lin T, Fan X, You H, Feng F. Inter-scanner reproducibility of brain volumetry: influence of automated brain segmentation software. *BMC Neurosci.* 2020;21(1):35.
- Wu J, Xia Y, Wang X, Wei Y, Liu A, Innanje A, Zheng M, Chen L, Shi J, Wang L, et al. uRP: an integrated research platform for one-stop analysis of medical images. *Front Radiol.* 2023;3:1153784.
- Piantino J, Boespflug EL, Schwartz DL, Luther M, Morales AM, Lin A, Fossen RV, Silbert L, Nagel BJ. Characterization of MR Imaging-visible Perivascular spaces in the White Matter of healthy adolescents at 3T. *AJNR Am J Neuroradiol.* 2020;41(11):2139–45.
- Jochims ACC, Blair GW, Stringer MS, Thrippleton MJ, Clancy U, Chappell FM, Brown R, Jaime Garcia D, Hamilton OKL, Morgan AG, et al. Relationship between venules and perivascular spaces in sporadic small Vessel diseases. *Stroke.* 2020;51(5):1503–6.
- Zhu YC, Tzourio C, Soumare A, Mazoyer B, Dufouil C, Chabriat H. Severity of dilated Virchow-Robin spaces is associated with age, blood pressure, and MRI markers of small vessel disease: a population-based study. *Stroke.* 2010;41(11):2483–90.
- George IC, Arrighi-Allisan A, Delman BN, Balchandani P, Horng S, Feldman R. A Novel Method to measure Venular Perivascular spaces in patients with MS on 7T MRI. *AJNR Am J Neuroradiol.* 2021;42(6):1069–72.
- Chen W, Song X, Zhang Y. Assessment of the Virchow-Robin Spaces in Alzheimer disease, mild cognitive impairment, and normal aging, using high-field MR imaging. *AJNR Am J Neuroradiol.* 2011;32(8):1490–5.
- Duperron MG, Tzourio C, Sargurupremraj M, Mazoyer B, Soumare A, Schilling S, Amouyel P, Chauhan G, Zhu YC, Debette S. Burden of Dilated Perivascular spaces, an emerging marker of Cerebral Small Vessel Disease. Is Highly Heritable Stroke. 2018;49(2):282–7.
- Doubal FN, MacLulich AM, Ferguson KJ, Dennis MS, Wardlaw JM. Enlarged perivascular spaces on MRI are a feature of cerebral small vessel disease. *Stroke.* 2010;41(3):450–4.
- Shi Y, Wardlaw JM. Update on cerebral small vessel disease: a dynamic whole-brain disease. *Stroke Vasc Neurol.* 2016;1(3):83–92.

25. Wei Z, Chen Q, Han S, Zhang S, Zhang N, Zhang L, Wang H, He Q, Cao P, Zhang X, et al. 5T magnetic resonance imaging: radio frequency hardware and initial brain imaging. *Quant Imaging Med Surg.* 2023;13(5):3222–40.
26. Zong X, Lian C, Jimenez J, Yamashita K, Shen D, Lin W. Morphology of perivascular spaces and enclosed blood vessels in young to middle-aged healthy adults at 7T: dependences on age, brain region, and breathing gas. *NeuroImage.* 2020;218:116978.
27. Feldman RE, Rutland JW, Fields MC, Marcuse LV, Pawha PS, Delman BN, Balchandani P. Quantification of perivascular spaces at 7T: a potential MRI biomarker for epilepsy. *Seizure.* 2018;54:11–8.
28. Cai K, Tain R, Das S, Damen FC, Sui Y, Valyi-Nagy T, Elliott MA, Zhou XJ. The feasibility of quantitative MRI of perivascular spaces at 7T. *J Neurosci Methods.* 2015;256:151–6.

Publisher's note

Springer Nature remains neutral with regard to jurisdictional claims in published maps and institutional affiliations.